ACS OMEGA

Open Access

http://pubs.acs.org/journal/acsodf

Article

Anti-Inflammatory Diterpenoids from the Aerial Parts of *Isodon suzhouensis*

Wen-Hu Liu,[#] Jin Chen,[#] Lan Wu,[#] Fu-Cai Ren, Xiang-Dong Pu, Bo-Yi Fan, Jing-Bo Shi,* and Chuan-Pu Shen*

Cite This: *ACS Omega* 2025, 10, 16658−16667

Read Online

ACCESS | Metrics & More | Article Recommendations | Supporting Information

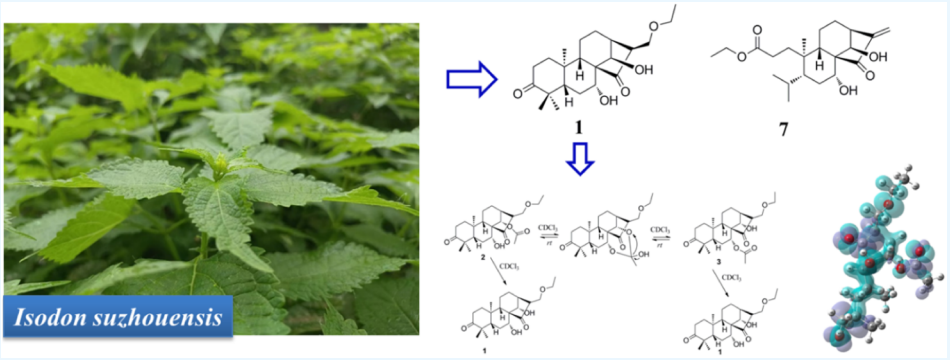

ABSTRACT: A phytochemical investigation of the aerial parts of *Isodon suzhouensis* resulted in the isolation of nine *ent*-kauranoid diterpenes, six of which were previously undescribed. The structures of these compounds were elucidated comprehensively using a combination of 1*D*/2D NMR spectroscopy and high-resolution electrospray ionization mass spectrometry (HRESIMS). Among the isolated compounds, compounds **2** and **3** exhibited intramolecular SN_2 tautomerism, a phenomenon further explained through the Fukui function and free energy calculations of the transition states of the reactions via the DFT calculation. Compound **7** is particularly noteworthy as it represents a novel case of C-3/C-4 carbon bond breakage in an *ent*-kauranoid diterpene, highlighting a unique structural modification in this class of natural products. All of the isolates were evaluated for their inhibitory effects on LPS-induced RAW 264.7 macrophages. Compound **8** emerged as a promising candidate, demonstrating significant inhibitory effects. Further studies confirmed that compound **8** suppresses the gene expression of the pro-inflammatory cytokines. The underlying anti-inflammatory mechanism of compound **8** was therefore investigated and shown to be related to the inhibition of the NF-κB signaling pathway activation.

1. INTRODUCTION

In China, plant-based beverages, often termed herb tea, are widely consumed for their health benefits.[1] In Suzhou City, located in northern Anhui Province of China, the aerial parts of *Isodon suzhouensis* (locally known as *Wangzaozi*) have been traditionally used as an herb tea for their antibacterial, anti-inflammatory, antitumor, antithrombotic, calming, and detoxifying properties.[2] Modern scientific research has corroborated these traditional uses, revealing that *Isodon suzhouensis* contains bioactive compounds with significant health benefits.[3]

The genus *Isodon*, belonging to the Labiatae family, is an important medicinal genus in China, comprising approximately 90 species and 21 variants. Extensive research on *Isodon* species has led to the isolation of numerous secondary metabolites,[3a,4] including *ent*-kauranoid diterpenes, which are considered characteristic components of this genus. These diterpenes feature a 6/6/6/5 tetracyclic skeleton and can undergo further oxygenation, ring-opening and ring-closing reactions to generate more complex and biologically active compounds.[3a,4]

Despite extensive research on *Isodon* plants, the aerial parts of *Isodon suzhouensis* have not been comprehensively investigated prior to this study. In our continuous research and exploration of anti-inflammatory Chinese herbal medicines,[5,6] we discovered that the extracts of aerial parts of *I. suzhouensis* exhibited promising anti-inflammatory activity. This prompted a comprehensive phytochemical investigation, leading to the isolation of six previously unreported *ent*-kauranoid diterpenes and three known ones, from the aerial parts of *Isodon suzhouensis* (Figure 1). Furthermore, the anti-inflammatory activities of the isolates were evaluated based on their ability to

Received: January 14, 2025
Revised: April 2, 2025
Accepted: April 10, 2025
Published: April 18, 2025

https://doi.org/10.1021/acsomega.5c00223
ACS Omega 2025, 10, 16658−16667

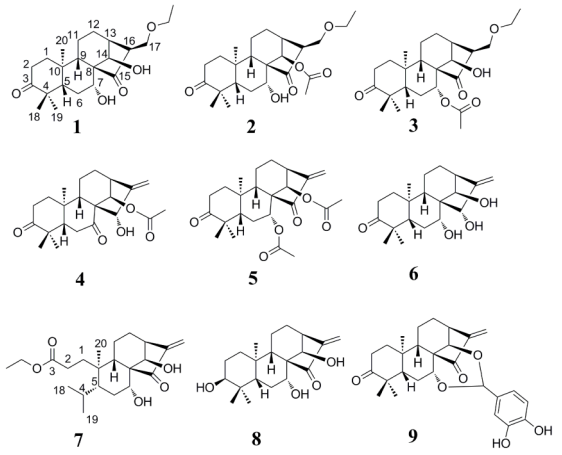

Figure 1. Diterpenes isolated from the aerial parts of *Isodon suzhouensis*.

inhibit nitric oxide (NO) in LPS-induced RAW264.7 macrophages. Additionally, the underlying mechanisms of their anti-inflammatory effects were explored.

2. EXPERIMENTAL SECTION

2.1. General Experimental Procedures. The absorbance measurements were conducted using a Shimadzu UV-1800 ultraviolet−visible spectrophotometer, while optical rotation was determined with an Anton Paar MCP 150 polarimeter. NMR spectra were recorded on a Bruker Avance III 500 NMR instrument (^{1}H: 500 MHz, ^{13}C: 125 MHz), with TMS as the internal standard. Mass spectra were recorded on a Dionex Ultimate 3000 UPLC-Q Exactive Plus (HR-ESI-MS). Silica gel (Qingdao Haiyang Chemical Co., Ltd., Qingdao, China), and RP-C18 (40−63 μm, Fuji, Japan) were used for column chromatography. Semipreparative HPLC was performed using a Thermo N3000 series instrument with a Thermo Scientific Hypersil GOLD DIM RP-C18 column (10 × 250 mm^2, 4.6 μm) or a Shimadzu LC-20AR series instrument with a Shim-pack RP-C_{18} column and an SPD-20A variable-wavelength detector.

2.2. Plant Material. The aerial parts of *Isodon suzhouensis* were collected from Yongqiao District, Suzhou City, Anhui Province, China, and identified by Zhengbin Han from Suzhou Lvyuan Traditional Chinese Medicine Technology Co., Ltd. A voucher specimen (No. 20220920) was deposited in the School of Pharmacy, Anhui Medical University.

2.3. Isolation and Purification. The dried aerial parts of *Isodon suzhouensis* (15.0 kg) were powdered and successively extracted by using 95% ethanol (v/v) for 6 times, each time for 24 h, in room temperature. After the removal of the solvents, the dried residue (1326 g) was partitioned successively by petroleum ether (PE) and ethyl acetate (EA). The EA-soluble

Table 1. ^{1}H and ^{13}C NMR Spectroscopic Data for Compounds 1−4

	1		2		3		4	
No.	δ_C	δ_H	δ_C	δ_H	δ_C	δ_H	δ_C	δ_H
1	29.1	1.90, m	29.3	1.78, m	26.5	1.78, m	39.4	2.90, t (14.0)
		1.27, m		1.28, m		1.28, m		
2	33.1	2.53, m	33.5	2.53, m	33.4	2.53, m	34.9	2.74, m
		2.42, m		2.42, m		2.42, m		2.45, m
3	216.2		216.5		216.3		217.7	
4	46.3		46.6		46.7		48.6	
5	51.3		51.1	1.68, m	52	1.84, m	53.9	1.80, d (2.7)
6	38.1	1.88, m	38.2	1.88, m	40.5	1.88, m	39.4	1.51, m
		1.35, m		1.35, m		1.35, m		
7	73.2	4.18, d (12.0)	73.1	4.06, dd (3.0, 12.0)	75.1	5.27 dd (3.5, 12.0)	210.1	
8	61.0		60.9		61.3		65.0	
9	53.5	1.28, m	53.3	1.30 m	54.7	1.42, m	49.8	2.17, d (8.2)
10	38.2		38.6		38.6		39.4	
11	24.9	1.83, m	24.8	1.83, m	24.7	1.83, m	34.9	2.74, m
								2.47, m
12	18.4	1.52, m	18.2	1.58, m	18.1	1.29, m	34.1	2.09, m
		1.27, m						1.77, m
13	49.6	3.23, m	50.1	3.09, m	49	3.21, m	47.1	2.78, brs
14	74.7	4.93, s	76.5	6.02, s	74.3	4.90, s	79.4	5.54, s
15	218.7		217.6		216.5		73.4	5.31, brt (2.5)
16	40.5	2.68, m	38.5	2.78, m	39.8	2.72, m	154.9	
17	66.0	3.86, m	66.2	3.53, 3.88 (overlapped)	66.2	3.52, 3.88 (overlapped)	108.4	5.10, s
		3.54, m						5.24, m
18	18.4	1.07, s	18.2	1.07, s	18.2	1.06, s	21.3	1.05, s
19	27.9	1.12, s	27.7	1.10, s	27.6	1.07, s	26.1	1.08, s
20	21.1	1.06, s	20.6	1.07, s	20.8	1.04, s	17.0	1.48, s
OCH_2CH_3	66.1	3.55, dt (9.5, 7.0)	66.5	3.55,(overlapped)	66.4	3.55, (overlapped)		
				3.48,(overlapped)		3.48, (overlapped)		
OCH_2CH_3	15.4	1.19, t (7.0 Hz)	15.1	1.19, (overlapped)	15.1	1.18, (overlapped)		
$OCOCH_3$			170.3		168.2		172.2	
$OCOCH_3$			21.3	2.04, s	21.5	2.03, s	20.8	1.92, s

https://doi.org/10.1021/acsomega.5c00223
ACS Omega 2025, 10, 16658−16667

Table 2. ^{1}H and ^{13}C NMR Spectroscopic Data for Compounds 5−7

No.	5		6		7	
	δ_C	δ_H	δ_C	δ_H	δ_C	δ_H
1	38.8	1.99, m	40.2	2.00, m	33.9	1.74, m
		1.32, m		1.48, m		
2	34.5	2.62, ddd (5.5, 9.4, 16.0)	34.9	2.44, m	29.5	2.12, m
		2.43, ddd (7.5, 8.0, 16.0)		2.56, m		2.03, m
3	219.3		220.4		176	
4	47.8		47.8		26.6	1.94, m
5	52.6	1.87, s	52.7	1.66, m	46.6	1.31, m
6	18.9	1.70, m	31.8	1.88, m	19	1.31, m
		1.49, m		1.78, m		1.65, m
7	75.4	5.20, dd (3.5, 12.0)	75.6	3.73, dd (4.0, 11.7)	74.7	
8	62.5		54.5		62.2	
9	56.1	1.59, d (8.5)	48.2	1.63, m	47.8	3.01, m
10	40.3		39.3		43.1	
11	33.3	2.20, m	28.1	2.03, m	29.5	2.01, m
		1.88, m		1.11, m		1.74, m
12	26.7	2.00, m	33.5	1.81, m	32.2	1.97, m
		1.74, m		1.58, m		1.76, m
13	45.7	3.13, s	50.5	2.58, m	47.5	1.39, m
14	76.2	6.01, s	77.9	4.50, s	76.8	4.83, s
15	205.5		73.4	5.06, m	208.9	
16	147.7		157.5		149.8	
17	118.2	6.08, s	108.1	5.24, s	117.9	6.08, s
		5.48, s		5.07, s		5.40, s
18	28.0	1.10, s	28	1.11, s	25	0.97 d (7.0 Hz)
19	21.4	1.04, s	21.5	1.08, s	19.1	0.89 d (7.0 Hz)
20	18.8	1.23, s	18.7	1.06, s	22.2	1.03, s
7-O$\underline{CO}CH_3$	171.7					
7−OCO$\underline{CH_3}$	21.3	1.74, s				
14-O$\underline{CO}CH_3$	172.4					
14−OCO$\underline{CH_3}$	21.3	2.03, s				
3-O$\underline{CH_2}CH_3$					61.8	4.07, q (7.0)
3-OCH$_2\underline{CH_3}$					14.6	1.22, t (7.0)

fraction (550 g) was subjected to a silica gel column chromatography (CC, 100 × 700 mm^2), gradient eluting by using PE-EA (100:1−50:1−25:1−10:1−5:1−3:1−1:1, v/v) to obtain seven fractions (Fr.A−Fr.G). Fr.D (30 g) was subjected to silica gel CC to obtain three subfractions, Fr.D1−Fr.D3, eluting with PE-EA (100:1−50:1−25:1−10:1−5:1−3:1−1:1, v/v). Fr.D2 was subjected to MCI gel column chromatography to obtain nine subfractions, Fr.D2-1−Fr.D2-9. Fr.D2-8 (556.9 mg) was subjected to repeated silica gel CC, Sephadex LH-20, and semipreparative HPLC to afford **2**/**3** (12.6 mg), **9** (6.0 mg), and **8** (15.1 mg). Fr.E (27.0 g) was subjected to MCI gel CC to obtain 8 subfractions, Fr.E1−Fr.E8. Compounds **1** (11.5 mg) and **4** (20.7 mg) were purified from Fr.E6 (243.5 mg) by using semipreparative HPLC. Fr.E7 (852.4 mg) was subjected to repeated silica gel CC, Sephadex LH-20, and semipreparative HPLC to afford compound **5** (11.9 mg). Fr.F (27.0 g) was also subjected to MCI gel CC to obtain 8 subfractions, Fr.F1−Fr.F8. Compounds **6** (3.8 mg) and 7 (2.8 mg) were purified by using semipreparative HPLC from Fr.F3 (127.3 mg).

2.4. Spectroscopic Data of Compounds. *Wazonin A* (**1**): white, amorphous powder. $[\alpha]_D^{20}$ −40.6° (*c* 0.65, MeOH); UV (MeOH) λ_{Max} (log ε) 191 (2.80), 235 (2.24) nm; ^{1}H and ^{13}C data ($CDCl_3$) see Table 1; HRESIMS *m*/*z* [M + Cl]$^-$ 413.2105 (calcd for $C_{22}H_{34}O_5$,413.2089).

Wazonin C (**4**): colorless, amorphous powder. $[\alpha]_D^{20}$ −0.30° (*c* 0.66, MeOH); UV (MeOH) λ_{Max} (log ε) 201 (2.37), 195 (2.06). ^{1}H and ^{13}C data (CD_3OD) see Table 1; HRESIMS *m*/*z* [M + Na]$^+$ 397.1984 (calcd for $C_{24}H_{36}O_6$, 397.1985).

Wazonin D (**5**): colorless, amorphous powder. $[\alpha]_D^{20}$ −1.65° (*c* 1.94, MeOH); UV (MeOH) λ_{Max} (log ε) 192 (3.35), 236 (1.65) nm. ^{1}H and ^{13}C data (CD_3OD) see Table 2; HRESIMS *m*/*z* [M + Na]$^+$ 439.2090 (calcd for $C_{24}H_{36}O_6$, 439.2091).

Wazonin E (**6**): colorless amorphous powder. $[\alpha]_D^{20}$ −0.21° (*c* 1.90, MeOH); UV (MeOH) λ_{max} (log ε) 208 (3.35), 200 (3.08) nm. ^{1}H and ^{13}C data (CD_3OD) see Table 2; HRESIMS *m*/*z* [M + Na]$^+$ 357.2035 (calcd for $C_{22}H_{30}O_5$, 357.2036).

Wazonin F (**7**): white, amorphous powder. $[\alpha]_D^{20}$ −13.33° (*c* 0.09, MeOH); UV (MeOH) λ_{Max} (log ε) 192 (3.34), 234 (1.91) nm. ^{1}H and ^{13}C data (CD_3OD) see Table 2; HRESIMS *m*/*z* [M + Na]$^+$ 401.2294 (calcd for $C_{24}H_{32}O_6$,401.2298).

2.5. Theoretical Calculations for Fukui Function and Free Energy. The density functional theory (DFT) method was conducted by using the Gaussian16 program. The B3LYP/6-31G(d,p) theoretical model was applied for all of the calculations. A potential energy surface scan was performed for Reaction 1, identifying the transition state and calculating the energy barrier. For Reaction 2, the QST1 method was used to locate the transition state, with the reactants and products

https://doi.org/10.1021/acsomega.5c00223
ACS Omega 2025, 10, 16658−16667

verified through IRC calculations to determine the energy barrier.

2.6. Cell Culture. The RAW 264.7 macrophage cell line was obtained from the Cell Bank of the Shanghai Institute of Biochemistry and Cell Biology, Chinese Academy of Sciences (Shanghai, People's Republic of China), and cultured in Dulbecco's Modified Eagle Medium (DMEM, Gibco Invitrogen Corp., Carlsbad, CA, USA). The cells were supplemented with 3.0 mM glutamine, antibiotics (100 U/mL penicillin and 100 U/mL streptomycin), and 10% heat-inactivated fetal bovine serum, and then maintained at 37 °C in a humidified atmosphere of 5% CO_2. For all experiments, macrophages were incubated in the presence or absence of various test compound concentrations, which were solubilized in DMSO and added 1 h prior to LPS (1.0 μg/mL) stimulation.

2.7. NO Production Tests. RAW 264.7 macrophage cells were seeded into 96-well plates at a density of 2×10^4 cells/mL and incubated with or without LPS (1.0 μg/mL) in the absence or presence of various isolate concentrations for up to 24 h. L-NMMA was used as a positive control. Nitrite accumulation in the supernatant was measured using the Griess reaction. Each 50 μL of culture supernatant was mixed with an equal volume of Griess reagent (0.1% naphthylethylenediamine, 1.0% sulfanilamide in 2.5% phosphoric acid solution) and incubated at room temperature for 10 min. Absorbance at 550 nm was measured using an automated microplate reader, and NO concentrations were determined from a sodium nitrite standard curve.

2.8. Real-Time Quantitative PCR. Following the manufacturer's instructions, total RNA was extracted from the cells using an RNA-Quick Purification Kit (GOONIE, 400−100). The premix was reverse-transcribed using an Evo-M-MLV (AG11706) and SYBR Green Pro Taq HS Pre-Mix qPCR Kit (AG11701) for reverse transcription and quantitative fluorescence PCR. For the quantitative polymerase chain reaction study, a CFX Connect Real-Time System (BIO-RAD) was used. Primers for TNF-α, IL-1β, and IL-6 genes were obtained from Sangon Biotech. GAPDH expression levels were used to normalize the transcript levels.

2.9. Western Blotting Assays. Total protein was extracted from the lysate of RAW 264.7 macrophage cells, and the protein content was determined using the BCA method. Protein samples were subjected to SDS-PAGE electrophoresis and then transferred onto PVDF membranes. The membranes were blocked with 5% skim milk at room temperature for 2 h and incubated with relevant primary antibodies (1:1000 dilution). After being rinsed with TBST, the membranes were incubated with the secondary antibody (1:500 dilution) conjugated with horseradish peroxidase. Following another rinse with TBST, the membranes were developed with an enhanced chemiluminescence (ECL) reagent. The optical density of the primary bands was measured using grayscale imaging software (UVP, UK) to calculate the protein expression levels.

2.10. Statistical Analysis. All data are expressed as means ± SEM. Statistical differences between data sets were analyzed by using GraphPad Prism 8 software. All experiments were repeated at least three times.

3. RESULTS AND DISCUSSION

Compound **1** (Wazonin A), a white amorphous compound, was assigned a molecular formula of $C_{22}H_{34}O_5$, based on the HR-ESI-MS $[M + Cl]^-$ ion peak observed at m/z 413.2105 (calcd 413.2089), indicating 6° of unsaturation. The ^{1}H NMR spectrum of **1** revealed characteristic signals, including three singlet methyl group signals (δ_H 1.07, 1.12, and 1.06), two oxygenated methine signals (δ_H 4.18, d, J = 12.0 Hz, and 4.93, s), and a set of ethoxyl group signals (δ_H 3.55, dq, J = 9.5, 7.0 Hz; 3.48, dq, J = 9.5, 7.0 Hz, and 1.19, t, J = 7.0 Hz). The ^{13}C NMR spectrum indicated 22 carbon resonances, including two carbonyl carbon signals (δ_C 219.1 and 216.6) and four oxygenated carbon signals (δ_C 74.5, 75.4, 66.6, and 66.7). The ^{13}C NMR spectrum exhibited 22 carbon resonances, featuring two carbonyl carbons (δ_C 219.1 and 216.6) and four oxygenated carbons (δ_C 74.5, 75.4, 66.6, and 66.7). Among the 6° of unsaturation, two were attributed to one olefinic bond and two carbonyl groups, suggesting a tetracyclic skeleton for **1**. The planar structure of **1** was elucidated through a detailed analysis of the HMBC spectrum. Key correlations included H-5, H_3−18 and H_3−19 to C-2; H-7 to C-14 and C-15; H-14 to C-13, C-15, and C-16; H-16 to C-13 and C-14; and H-17 to C-15, which positioned the two carbonyl groups at C-2 and C-15, respectively. Additionally, three oxygenated groups were assigned to C-7, C-14, and C-17. The HMBC correlation of H_2−O$\underline{CH_2}$$CH_3$ to C-17 confirmed the attachment of the ethoxy group at C-17. The relative structure of compound **1** was determined by NOESY correlations. The NOESY correlations of H_3-18 to H-5 and H_3-20 to H_3-19 indicated the A/B-trans conformation of rings A and B. Meanwhile, the NOESY correlation between H-14 and H_3-20, and H-5 and H-7 revealed 14β−OH and 7α−OH, respectively. Meanwhile, H_2−O$\underline{CH_2}$$CH_3$ to H-16 and H-13 to H-17 correlations assigned 17-methylene as the β-orientation.

Compound **2** was isolated as a colorless, amorphous powder. To elucidate its chemical structure, we initially tested its NMR spectra in $CDCl_3$. Interestingly, after approximately 24 h of exposure to natural light at room temperature, the NMR analysis revealed that the single compound had undergone conversion into three distinct compounds (**1**, **2**, and **3**). The resulting mixture was further characterized using ^{13}C NMR, HSQC, and HMBC spectra (Figure 2). Unfortunately, due to

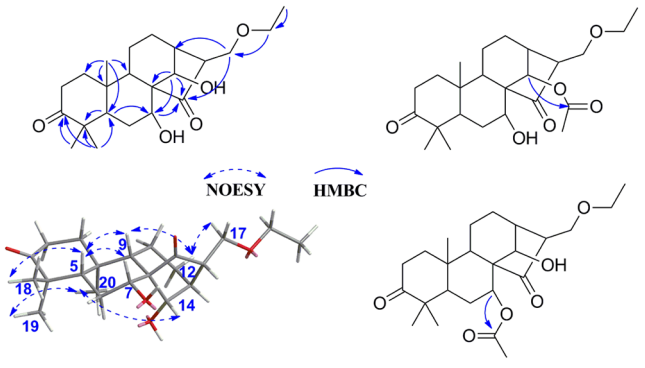

Figure 2. Key HMBC and NOESY correlations of **1**−**3**.

the considerable distance between the testing site and our laboratory, the sample was lost during transportation from Guilin to Hefei. This loss prevented us from repurifying the sample or exploring the effect of different NMR solvents on the conversion process. With only a minimal amount of the sample remaining (<1.0 mg), we were limited to simulating its behavior in $CDCl_3$ and obtaining retention time data for the

https://doi.org/10.1021/acsomega.5c00223
ACS Omega 2025, 10, 16658−16667

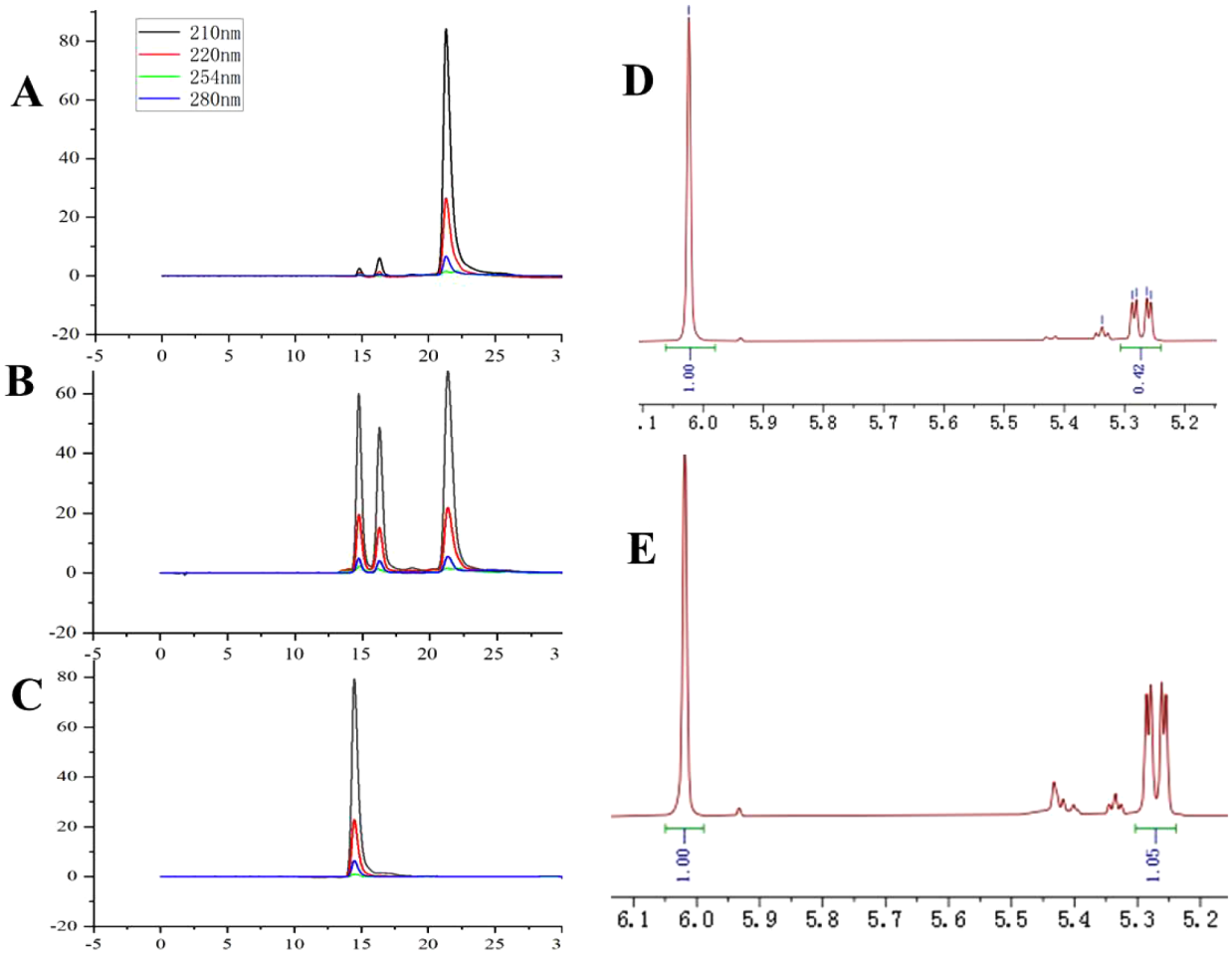

Figure 3. (A) The immediate HPLC analysis of compound **2**; (B) the HPLC analysis result of compound **2** after the long time NMR tests; (C) the HPLC analysis of compound **1**; (D) the NMR test result of **2** in 06/05/2023; (E) the NMR test result of **2** in 07/19/2023.

conversion products (Figure 3). The complexity of the mixture's spectrum initially hindered further structural analysis. However, in December 2023, we were fortunate enough to obtain compound **1**, which was confirmed to be one of the mixtures through comparison of HPLC and NMR spectroscopic data. Inspired by the structure of compound **1**, we successfully elucidated the structures of **2** and **3**.

Compounds **2** and **3** (wazonin B) share a molecular formula of $C_{24}H_{36}O_6$, as deduced from the $[M + Na]^+$ ion peak observed at m/z 443.2407 (calcd 443.2404). In the ^1H NMR spectrum, the ratio of compounds **2** and **3** was changed from 1:0.4 at the initial time for 1D NMR testing (2023/06/05) to 1:1.06 one month later for 2D NMR testing (2023/07/19). The ^1H NMR spectrum displayed three sets of signals corresponding to ent-kauranoid diterpenes, along with two distinct acetyl signals (δ_H 2.04 and 2.03), confirming that **2** and **3** are acetylated diterpenoid derivatives. The data from the ^{13}C NMR spectrum of the mixture revealed the three copies of the data of **1**, except the additional acetyl carbonyl signals (δ_C 170.3 and 168.2). Further HMBC correlation of the mixture confirmed that these compounds have very similar planar structures. The HMBC correlation of H-14 to C-$\underline{CO}CH_3$ in **2** and H-7 to C-$\underline{CO}CH_3$ in **3** built the planar structures of **2** and **3**, respectively (Figure 2). Based on these findings, we have found that compound **1** is the product of acetyl hydrolysis of compounds **2** and **3**. This phenomenon reminds us of three sets of compounds found by our team in *Isodon amethystoides* of the same genus.[7] For example, the acetyl compounds glaucocalyxins B and D undergo mutual transformation; meanwhile, glaucocalyxins B and D can also undergo acetyl hydrolysis in a $CDCl_3$ solution. Through the analysis of compounds **1**-**3**, we can find that similar phenomena also exist in compounds **1**-**3**. Due to the fact that only hydrolysis reaction occurred, the configuration of compounds **1**-**3** remains consistent. We assigned the NMR data of **2** and **3** with the help of NMR spectra. Compound **3** was given the trivial name wazonin B. Compound **2** (glaucocalyxin R) was just reported as a single compound from the roots of *Isodon japonica* var. *glaucocalyx*.[8] However, careful examination of the original spectrum of glaucocalyxin R suggests that it was not obtained in pure form, likely due to interconversion between compounds, similar to the behavior observed in **2** and **3**.

Due to the limitation of compound quantity, we are unable to directly observe the transformation process. However, the conversion between **2** and **3** is proposed to proceed via an intramolecular SN_2 reaction mechanism (Figure 4). We employed DFT calculations to explain the underlying mechanism. Therefore, the Fukui function and free energy of the reaction were calculated. In the Fukui function results of **2**, as depicted in Figure 4, the groups marked in green indicate that the position is prone to electrophilic reactions, while the groups marked in purple indicate that the position is prone to nucleophilic reactions. In the molecule of compound **2**, the acetyl group at C-14 is highly susceptible to nucleophilic

https://doi.org/10.1021/acsomega.5c00223
ACS Omega 2025, 10, 16658−16667

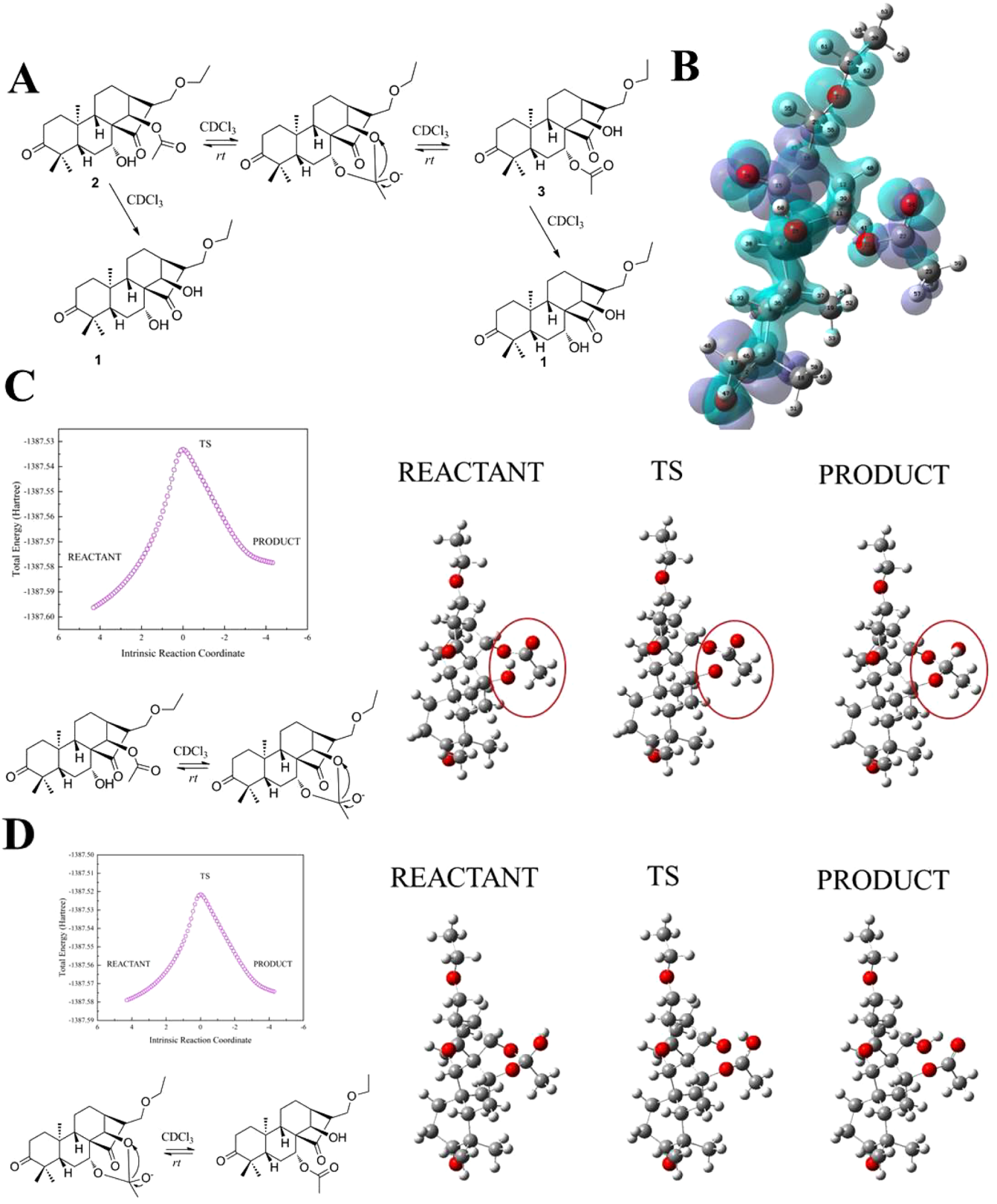

Figure 4. (A) The proposed tautomeric reaction among compounds **1**, **2** and **3**. (B) The result of DFT calculation of fukui function, Oribtical-weighted f+ (purple) for nucleophilic reactions oribtical-weighted f-(green) for electrophilic reaction. (C) The DFT calculation result of free energy of reaction **1** (TS for transition state). (D) The DFT calculation result of free energy of reaction **2** (TS for transition state).

reactions, while the 7-hydroxyl group is also highly susceptible to electrophilic reactions. Therefore, this reaction is dependent on its occurrence. In Figure 3A, the purified compound **2** was immediately analyzed via HPLC. Two impurities (compounds **1** and **3**) were found in relatively small quantities in the regions with high polarity. This means that during the solvent recovery

https://doi.org/10.1021/acsomega.5c00223
ACS Omega 2025, 10, 16658−16667

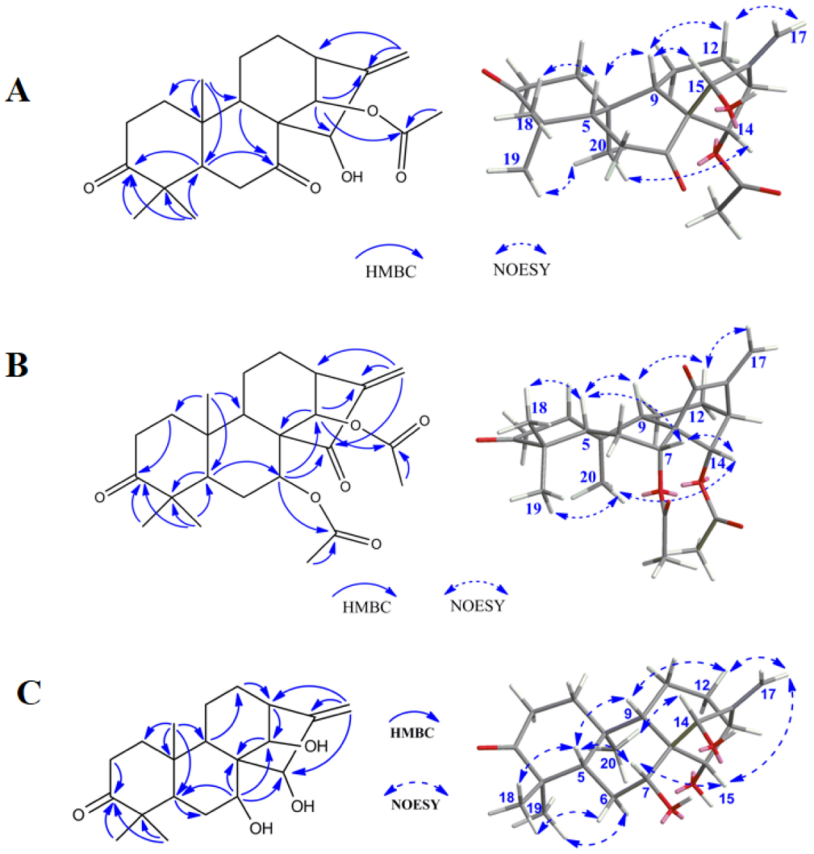

Figure 5. Key HMBC and NOESY correlations of (A) **4**, (B) **5**, and (C) **6**.

process, heating (40 °C) can cause a slight transformation of compound **2** in neutral solvents (CH_3OH-H_2O, 60:40, v/v). Subsequent NMR testing revealed that the sample was dissolved in $CDCl_3$ and exposed to natural light at room temperature. The results showed that the conversion efficiency of compound **2** accelerates in this environment. Therefore, compound **2** can undergo transformation under trace heating conditions and the weak acid environment provided by $CDCl_3$. To further explain this phenomenon, we explored the mechanism of the reaction using DFT calculations. As shown in Figure 4C,D, for reaction 1, the energy gap between compound **2** and the immediate phase was 238.7 kJ/mol (57.0 kcal/mol). For reaction 2, the energy gap between compound **2** and the immediate phase was 134.8 kJ/mol (32.2 kcal/mol). By calculation, the free energy gaps of the two reactions are relatively high, so a certain amount of energy needs to be provided by the outside world. This validates our findings during the purification and testing process. Due to the limitation of amount, we did not use ultralow-temperature NMR testing to verify the effect of temperature on the reaction. In our previous research on *Isodon amethystoides* of the same genus, we found that the mutual transformation of compounds wangzaozitones A and B stopped at a temperature of −15 °C.[7] The reaction mechanism of these compounds is interesting and deserves further exploration.

Compound **4** (wazonin C) was obtained as an amorphous powder. Its molecular formula was determined to be $C_{22}H_{30}O_5$ based on the HRESIMS ion peak $[M + Na]^+$ observed at 397.1984 (calcd 397.1985). The ^1H NMR spectrum of **4** indicated three singlet methyl signals (δ_H 1.05, 1.08, 1.48, and 1.92), a pair of terminal olefinic protons (δ_H 5.24 and 5.10), and two oxygenated methine protons (δ_H 5.54 and 5.31). The ^{13}C NMR revealed 22 carbon signals, comprising carbonyl carbon signals (δ_C 210.1 and 217.7), two oxygenated carbon resonances (δ_C 73.4 and 79.7), an acetyl carbon signal (δ_C 172.2), and two olefinic carbon signals (δ_C 154.9 and 108.4). These NMR data suggested that **4** is an ent-kaurane diterpene, structurally similar to compound **1** but distinguished by the presence of an additional acetyl group. The HMBC correlations of H-5, H-9, and H-14 to C-7 suggested the C-7 carbonyl group, while correlations of H-14 to C-$\underline{CO}CH_3$ and C-16 suggested the additional acetyl group at C-14. The relative configuration of **4** was confirmed by NOESY correlations of H_3-19 and H-14 to H_3-20, H_3-18 to H-5 and H-5 to H-9, H-9 to H-12a and H-15, and H-12a to H-17.

Compound **5** (wazonin D) was also an *ent*-kauranoid diterpene with a molecular formula $C_{24}H_{32}O_6$, deduced from the HRESIMS spectrum of the $[M + Na]^+$ ion peak observed at 439.2090 (calcd. 439.2091). The ^1H and ^{13}C NMR spectra indicated that compound **5** had a structure similar to that of the known compound glaucocalyxin B, except for an additional acetyl group. The HMBC correlation of H-7 and H-14 to C-$COCH_3$ suggested that compound **5** was a diester diterpenoid. The relative configuration of **5** was determined by the NOESY correlations of H-14 and H_3-19 to H_3-20, H_3-18 to H-5 and H-5 to H-9, H-9 to H-12a and H-15, and H-12a to H-17 (Figure 5).

Compound **6** (wazonin E) was found to have a molecular formula of $C_{20}H_{30}O_4$ as evidenced by HR-ESI-MS (m/z 357.2035 $[M + Na]^+$, calcd for 357.2036). The ^1H NMR spectra of **6** indicated three singlet methyl groups (δ_H 1.08, 1.11, and 1.06), three oxygenated methine proton signals (δ_H

https://doi.org/10.1021/acsomega.5c00223
ACS Omega 2025, 10, 16658−16667

4.50, s, 5.06, s, and 3.73, dd, J = 4.0, 11.7 Hz), and a pair of terminal olefinic proton signals (δ_H 5.24, s and 5.07, s). The ^{13}C NMR and HSQC spectra resolved 20 carbon resonances, including one carbonyl carbon signal (δ_C 220.4), two olefinic carbon signals (δ_C 157.5 and 108.1), and three oxygenated carbon signals (δ_C 77.9, 75.6, and 73.4). The aforementioned data revealed **6** have a similar structure with that of wangzaozilactone A,[7] except the absence of an acetyl group in **6**. Further HMBC correlations of H-17 to C-15 and C-13, H-14 to C-16 and C-15, and H-7 to C-14 and C-15 built the trihydroxyl group. The relative structure of **6** was elucidated by NOESY correlations of H_3-19 and H-14 to H_3-20, H_3-18 to H-5 and H-5 to H-9, H-9 to H-12a and H-15, and H-12a to H-17.

Compound **7** (wazonin F) had a molecular formula $C_{22}H_{34}O_5$ deduced from the HRESIMS $[M + Na]^+$ ion peak observed at 401.2294 (calcd 401.2298), corresponding to 6° of unsaturation. The ^{1}H NMR spectrum revealed one singlet methyl group (δ_H 1.03), two doublet methyl groups (δ_H 0.97, d, J = 7.0 Hz and 1.06, d, J = 7.0 Hz), one set of terminal olefinic proton signals (δ_H 6.08, s and 5.40, s), one set of ethyl group (1.22, t, J = 7.0 Hz and 4.07, q, J = 7.0 Hz) and two oxygenated methines (δ_H 4.83, s and 4.02, dd, J = 12.0, 4.0 Hz). The ^{13}C NMR combined with the HSQC resolved 22 carbon resonances, including one carbonyl carbon (δ_C 208.9), one ester carbonyl carbon (δ_C 176.0), two oxygenated carbon signals (δ_C 74.7 and 74.9), and two olefinic carbon resonances (δ_C 117.9 and 149.8). It can be indicated that **7** is a tricyclic terpenoid, with three of the six unsaturations accounted for by double bonds. The remaining 20 carbons, excluding the ethoxyl group, suggest that compound **7** is a diterpenoid.

Through detailed analysis of ^{1}H−^{1}H COSY, HSQC, and HMBC spectra (Figure 6), a kauranoid-like moiety was

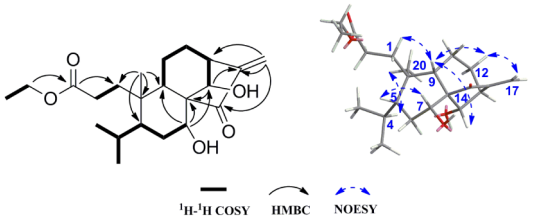

Figure 6. Key HMBC and NOESY correlations of **7**.

constructed in rings B, C, and D of compound **7**, consistent with the structural features of 7,14-dihydroxy *ent*-kaurane diterpenoids. Four spin coupling units, highlighted with bold bonds, were established by the ^{1}H−^{1}H COSY spectrum (Figure 6). The HMBC correlations of H-1 to C-3 and H_3-20 to C-1, C-5, C-10, and C-9, combined with spin coupling of H-18−H-4−H-19 and H-4−H-5−H-6, revealed the A ring of *ent*-kauranoid skeleton cleaved between C-3 and C-4. Further HMBC correlations, such as H-7 to C-9, C-8, and C-14, H-14 to C-8, C-16, and H-17 to C-13, C-16, and C-15, confirmed the connectivity of the remaining three rings. The H_2−OCH_2CH_3 to C-3 located the ethyl group at C-3. The relative configuration of **7** was determined using NOESY correlations from H_3-20 to H-4 and H-14, H-5 to H-7, H-1 to H-9, H-9 to H-12a, and H-12a to H-17. The absolute configuration of **7** was determined by an ECD calculation. Compound **7** was assigned the trivial name Wazonin G and represents a rare example of a C-3/C-4 cleaved ent-kauranoid diterpene. A plausible biogenetic pathway for **7** is proposed in Scheme 1.

The remaining known compounds were isolated and elucidated as wangzaozin A (**8**)[9] and glaucocalyxin H (**9**),[10] respectively.

As a traditional anti-inflammatory medicinal herb, the aerial parts of *I. suzhouensis* have been widely used to treat pulmonary inflammatory diseases. During the progression of the disease, macrophages play a pivotal pro-inflammatory role,[11] primarily through the secretion of nitric oxide (NO).[12] Thus, all the isolates were evaluated for their inhibitory activities against the NO production of LPS-stimulated RAW 264.7 macrophages (Table 3). Among the tested compounds,

Table 3. Inhibitory Activities of Isolates on the LPS-Stimulated RAW264.7 Macrophages

NO.	NO inhibition IC_{50} (μM)
1	>50
4	21.24 ± 3.77
5	>50
6	>50
7	11.37 ± 2.30
8	3.05 ± 0.49
9	>50
L-NMMA	8.26 ± 2.60

compound **8** exhibited the most potent activity, with an IC_{50} value at 3.05 ± 0.49 μM. The overproduction of NO in the LPS-stimulated RAW 264.7 macrophages is always accompanied by the abnormal release of pro-inflammatory cytokines, including IL-1β, IL-6, and TNF-α.[13] The levels of gene expression for IL-1β, IL-6, and TNF-α were measured by QPCR. The results showed that compound **8** significantly down-regulated the expression of IL-1β, IL-6, and TNF-α in a dose-activity dependence relationship. These findings strongly suggest that **8** is a highly credible anti-inflammatory agent. The NF-κB signaling pathway plays a central role in regulating the

Scheme 1. Plausible Biogenetical Pathway of Compound 7

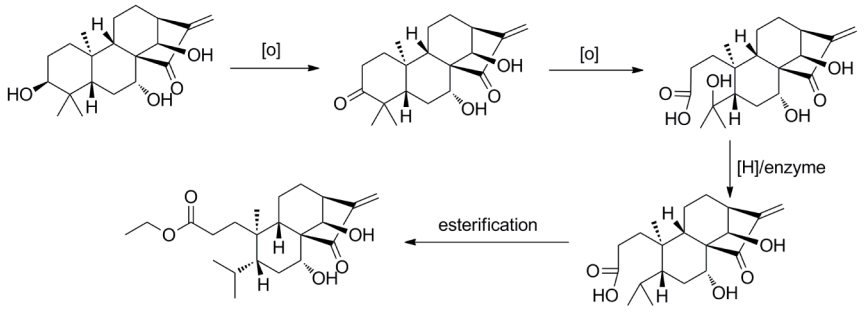

https://doi.org/10.1021/acsomega.5c00223
ACS Omega 2025, 10, 16658−16667

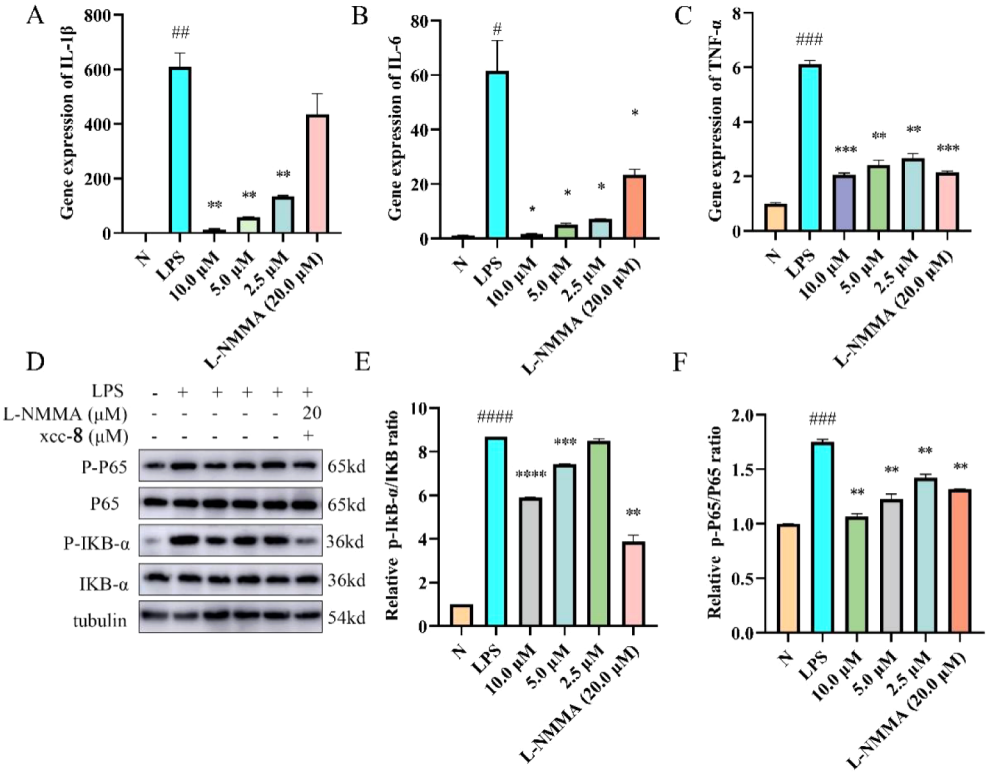

Figure 7. (A–C) IL-1β, IL-6, and TNF-α levels were measured by QPCR. (D) Western blotting results. Raw 264.7 macrophages were pretreated with the indicated concentrations of **8** for 1 h and then challenged with 1.0 μg/mL LPS for 24 h. The macrophages were collected and lysed for WB analysis on the expression of the canonical NF-κB pathway. Tubulin served as the loading control. (E,F) Relative p-IκB-α/IκB and p-P65/P65 ratio. Each bar represents the mean ± SEM in three independent experiments. $^{*}p < 0.05$, $^{**}p < 0.01$ vs the LPS group. $^{\#}p < 0.05$, $^{\#\#}p < 0.01$, $^{\#\#\#}p < 0.001$, $^{\#\#\#\#}p < 0.0001$ vs the normal group.

inflammatory cascade, including the production of pro-inflammatory cytokines and NO[13b,14] Therefore, we performed Western blot analysis to investigate the levels of phospho-IκB-α and phospho-NF-κB p65. As depicted in Figure 7, compound **8** significantly inhibited the activation of the NF-κB signaling pathway.

4. CONCLUSION

In conclusion, nine *ent*-kauranoids, including six previously unreported compounds, were isolated from the roots of *I. suzhouensis*. Among these, compounds **1**-**3** represent a type of compound with tautomerism properties and are hydrolyzed easily. The phenomenon was further confirmed by HPLC and NMR analyses, with additional insight provided by Fukui function and free energy calculations. *In vitro* biological activity assays revealed that compound **8** possesses significant anti-inflammatory potential, likely mediated through the inhibition of the activation of the NF-κB pathway. These findings not only enhance our understanding of the chemical diversity of *I. suzhouensis* but also highlight its potential as a source of novel anti-inflammatory agents for further development.

■ ASSOCIATED CONTENT

Supporting Information

The Supporting Information is available free of charge at https://pubs.acs.org/doi/10.1021/acsomega.5c00223.

Spectra, 1D and 2D NMR spectra for compounds **1**–**7** (PDF)

■ AUTHOR INFORMATION

Corresponding Authors

Jing-Bo Shi – *Anhui Provincial laboratory of inflammatory and immunity disease, Anhui Institute of Innovative Drugs, School of Pharmacy, Anhui Medical University, Hefei 230032, People's Republic of China*; Email: scp1001@126.com

Chuan-Pu Shen – *Anhui Provincial laboratory of inflammatory and immunity disease, Anhui Institute of Innovative Drugs, School of Pharmacy, Anhui Medical University, Hefei 230032, People's Republic of China*; orcid.org/0000-0001-6896-4541; Email: sjbo616@126.com

Authors

Wen-Hu Liu – *Anhui Provincial laboratory of inflammatory and immunity disease, Anhui Institute of Innovative Drugs, School of Pharmacy, Anhui Medical University, Hefei 230032, People's Republic of China*

Jin Chen – *Anhui Provincial laboratory of inflammatory and immunity disease, Anhui Institute of Innovative Drugs, School of Pharmacy, Anhui Medical University, Hefei 230032, People's Republic of China*

Lan Wu – *Anhui Provincial laboratory of inflammatory and immunity disease, Anhui Institute of Innovative Drugs, School of Pharmacy, Anhui Medical University, Hefei 230032, People's Republic of China*

Fu-Cai Ren – *Anhui Provincial laboratory of inflammatory and immunity disease, Anhui Institute of Innovative Drugs,*

https://doi.org/10.1021/acsomega.5c00223
ACS Omega 2025, 10, 16658–16667

School of Pharmacy, Anhui Medical University, Hefei 230032, People's Republic of China

Xiang-Dong Pu − *Anhui Provincial laboratory of inflammatory and immunity disease, Anhui Institute of Innovative Drugs, School of Pharmacy, Anhui Medical University, Hefei 230032, People's Republic of China;* orcid.org/0000-0002-0892-035X

Bo-Yi Fan − *School of Pharmacy, Nantong University, Nantong 226019, People's Republic of China;* orcid.org/0000-0003-1581-8422

Complete contact information is available at: https://pubs.acs.org/10.1021/acsomega.5c00223

Author Contributions

#W.-H.L., J.C., and L.W. equally contributed to this work The manuscript was written through contributions of all authors. All authors have given approval to the final version of the manuscript.

Notes

The authors declare no competing financial interest.

■ ACKNOWLEDGMENTS

This research work was supported by the Natural Science Project of the Anhui Provincial Education Department (2024AH050716 and 2022AH030078) and the Anhui Medical University Pharmacy Peak Discipline Project (2023xktdzy2). The authors also thank Dr. Sheng Wang from the Center for Scientific Research at Anhui Medical University for his valuable help with our experiment.

■ REFERENCES

(1) (a) Hou, Y.; Jiang, J. G. Origin and concept of medicine food homology and its application in modern functional foods. *Food Funct.* **2013**, *4* (12), 1727−1741. (b) Liu, F.; Su, Y.; Wu, J.; Zhou, Q.; Wang, M. Exploring the sensory acceptance, physicochemical properties, and phenolamide leaching characteristics of rose tea. *Food Chem.* **2025**, *463*, 141164. (c) Wang, Y.; Li, S.; Sun, J.; Li, Y.; Hu, Y.; Shen, C.; Liu, F.; Guo, S.; Chen, F.; Liu, Q.; et al. Comprehensive assessment for species authenticity, pesticide residual, and fungal contamination characteristics of Panax herbal tea. *LWT* **2024**, *207*, 116688.

(2) (a) Wang, W.; Li, H.; Lv, J. M.; Khan, G. J.; Duan, H.; Zhu, J.; Bao, N. N.; Zhai, K. F.; Xue, Z. L. Determination of the Anti-Oxidative Stress Mechanism of *Isodon suzhouensis* Leaves by Employing Bioinformatic and Novel Research Technology. *ACS Omega* **2023**, *8* (3), 3520−3529. (b) Zhai, K.; Wang, W.; Zheng, M.; Khan, G. J.; Wang, Q.; Chang, J.; Dong, Z.; Zhang, X.; Duan, H.; Gong, Z.; Cao, H. Protective effects of *Isodon Suzhouensis* extract and glaucocalyxin A on chronic obstructive pulmonary disease through SOCS3−JAKs/STATs pathway. *Food Front.* **2023**, *4* (1), 511−523. (c) Ma, H.; Zhai, K.; Han, Z.; Zhou, S. Isodon suzhouensis (Lamiaceae): A new species from Anhui. *J. Suzhou Uni* **2022**, *37* (3), 41−45.

(3) (a) Liu, M.; Wang, W.-G.; Sun, H.-D.; Pu, J.-X. Diterpenoids from Isodon species: an update. *Nat. Prod. Rep.* **2017**, *34* (9), 1090−1140. (b) Mu, L.; Li, T.; Wu, P.-L.; Cai, L.-Q.; Li, S.-Y.; Wang, Z.-Y.; Liu, Y.-Y.; Wang, J.; Yan, D.; Rao, Z.-Y.; Wang, C.-J.; Zhang, J.; Cao, Y.; Pan, K.; Yin, Z.-Q. 5-epi-ent-Kaurane diterpenoids from the aerial parts of *Isodon eriocalyx* and their anti-atherosclerotic potential. *Phytochemistry* **2023**, *209*, 113621. (c) Zhao, C.; Zhou, L.; Xie, W.; Zhao, L.; Zhang, C.; He, K.; Ye, J.; Zhang, J.; Pan, L.; Zou, J.; Zhang, H. Bioactive isopimarane and 3,4-seco isopimarane diterpenoids from *Isodon amethystoides*. *BMC Chem.* **2022**, *16* (1), 96. (d) Dai, J. M.; Yan, B. C.; Hu, K.; Li, X. R.; Li, X. N.; Sun, H. D.; Puno, P. T. Isoxerophilusins A and B, Two Novel Polycyclic Asymmetric Diterpene Dimers from *Isodon xerophilus*: Structural Elucidation, Modification, and Inhibitory Activities against α-Glucosidase. *Org. Lett.* **2024**, *26* (29), 6203−6208.

(4) Sun, H.-D.; Huang, S.-X.; Han, Q.-B. Diterpenoids from Isodon species and their biological activities. *Nat. Prod. Rep.* **2006**, *23* (5), 673−698.

(5) Yin, X.-W.; Zhang, M.; Wu, L.; Ren, F.-C.; Yang, F.-R.; Pu, X.-D.; Zhang, Z.-J.; Shen, C.-P. Anti-Inflammatory Peroxidized Chlorahololide-Type Dimers Are Artifacts of Shizukaol-Type Dimers: From Phenomena Discovery and Confirmation to Potential Underlying Mechanism. *Molecules* **2024**, *29* (4), 909.

(6) Yin, X. W.; Hu, J. J.; Ren, F. C.; Pu, X. D.; Yang, M. Y.; Yang, B. Y.; Wang, P.; Shen, C. P. Anti-inflammatory Lindenane Sesquiterpene Dimers from the Roots of *Chloranthus fortunei*. *ACS Omega* **2024**, *9* (32), 34869−34879.

(7) Wu, L.; Zhang, M.; Liu, W.-H.; Chen, Y.-F.; Yin, X.-W.; Han, Z.; Ren, F.-C.; Pu, X.-D.; Liu, X.-H.; Shi, J.-B.; Shen, C.-P. The intramolecular SN2 reaction tautomeric ent-Kauranoids isolated from the aerial parts of *Isodon amethystoides*. *Fitoterapia* **2024**, *173*, 105788−105788.

(8) Wang, G.; Ding, A.-X.; Qin, G.-Q.; Chen, T.; Hu, X.-G.; Zheng, L.; Du, G.-X.; Wang, W.; Xuan, L. Dimeric ent-kauranoids isolated from *Isodon japonica var. glaucocalyx* and their anti-inflammatory activities. *Fitoterapia* **2024**, *174*, 105840.

(9) Ding, L.; Yu, K.-B.; Liu, G.-A. Crystal structure for cytotoxic diterpenoids Wangzaozin A. *Chem. J. Chin. Univ.* **2005**, *26* (8), 1455−1458.

(10) Hai, G.; Zhang, C.; Jia, Y.; Bai, S.; Han, J.; Guo, L.; Cui, T.; Niu, B.; Huang, F.; Song, Y. Anti-hepatoma activity of a novel compound glaucocalyxin H in vivo and in vitro. *AAPS PharmScitech* **2015**, *16* (3), 496−504.

(11) Shi, T.; Denney, L.; An, H.; Ho, L.-P.; Zheng, Y. Alveolar and lung interstitial macrophages: Definitions, functions, and roles in lung fibrosis. *J. Leukocyte Biol.* **2021**, *110* (1), 107−114.

(12) (a) Li, Q. M.; Luo, J. G.; Wang, X. B.; Yang, M. H.; Kong, L. Y. Sesquiterpenes from the rhizomes of *Alpinia japonica* and their inhibitory effects on nitric oxide production. *Fitoterapia* **2013**, *86*, 29−34. (b) Lou, T.; Jiang, W.; Xu, D.; Chen, T.; Fu, Y. Inhibitory Effects of Polydatin on Lipopolysaccharide-Stimulated RAW 264.7 Cells. *Inflammation* **2015**, *38* (3), 1213−1220.

(13) (a) Shen, C.-P.; Luo, J.-G.; Yang, M.-H.; Kong, L.-Y. Cafestol-Type Diterpenoids from the Twigs of *Tricalysia fruticosa* with Potential Anti-inflammatory Activity. *J. Nat. Prod.* **2015**, *78* (6), 1322−1329. (b) Wang, J.; Liu, Y.-T.; Xiao, L.; Zhu, L.; Wang, Q.; Yan, T. Anti-Inflammatory Effects of Apigenin in Lipopolysaccharide-Induced Inflammatory in Acute Lung Injury by Suppressing COX-2 and NF-kB Pathway. *Inflammation* **2014**, *37* (6), 2085−2090.

(14) (a) Chen, Z.; Zhang, X.; Chu, X.; Zhang, X.; Song, K.; Jiang, Y.; Yu, L.; Deng, X. Preventive effects of valnemulin on lipopolysaccharide-induced acute lung injury in mice. *Inflammation* **2010**, *33* (5), 306−314. (b) Pahl, H. L. Activators and target genes of Rel/NF-kappaB transcription factors. *Oncogene* **1999**, *18* (49), 6853−6866.